crystals

MDPI

Article

Simple Approach to Medical Grade Alumina and Zirconia Ceramics Surface Alteration via Acid Etching Treatment

Damian Stanislaw Nakonieczny [1,2], Aleš Slíva [3], Zbigniew Paszenda [2], Marianna Hundáková [1], Gabriela Kratošová [1], Sylva Holešová [1], Justyna Majewska [4], Piotr Kałużyński [5], Sajjan Kumar Sathish [1] and Gražyna Simha Martynková [1,*]

1 Nanotechnology Centre, CEET, VŠB-Technical University of Ostrava, 17, Listopadu 15/2172, 708 00 Ostrava, Czech Republic; damian.nakonieczny@polsl.pl (D.S.N.); marianna.hundakova@vsb.cz (M.H.); gabriela.kratosova@vsb.cz (G.K.); sylva.holesova@vsb.cz (S.H.); sajjan56@gmail.com (S.K.S.)
2 Department of Biomedical Engineering, Silesian University of Technology, Akademicka 2A, 44-100 Gliwice, Poland; Zbigniew.Paszenda@polsl.pl
3 Institute of Transport, Faculty of Mechanical Engineering, VŠB-Technical University of Ostrava, 17, Listopadu 15/2172, 708 00 Ostrava, Czech Republic; ales.sliva@vsb.cz
4 Department of Biosensors and Biomedical Signal Processing, Silesian University of Technology, Akademicka 2A, 44-100 Gliwice, Poland; justyna.majewska@polsl.pl
5 Department of Optoelectronics, Silesian University of Technology, Akademicka 2A, 44-100 Gliwice, Poland; piotr.kaluzynski@polsl.pl
* Correspondence: grazyna.simha@vsb.cz; Tel.: +420-596991572

check for updates

Citation: Nakonieczny, D.S.; Slíva, A.; Paszenda, Z.; Hundáková, M.; Kratošová, G.; Holešová, S.; Majewska, J.; Kałużyński, P.; Sathish, S.K.; Simha Martynková, G. Simple Approach to Medical Grade Alumina and Zirconia Ceramics Surface Alteration via Acid Etching Treatment. *Crystals* **2021**, *11*, 1232. https://doi.org/10.3390/cryst11101232

Academic Editor: Marilena Carbone

Received: 16 September 2021
Accepted: 9 October 2021
Published: 12 October 2021

Abstract: In order for bioceramics to be further used in composites and their applications, it is important to change the surface so that the inert material is ready to interact with another material. Medical grade alumina and zirconia ceramic powders have been chemically etched with three selected acidic mixtures. Powder samples were taken for characterization, which was the key to evaluating a successful surface change. Changes in morphology, together with chemical composition, were studied using scanning electron microscopy, phase composition using X-ray diffraction methods, and nitrogen adsorption/desorption isotherms are used to evaluate specific surface area and porosity. The application of HF negatively affected the morphology of the material and caused agglomeration. The most effective modification of ceramic powders was the application of a piranha solution to obtain a new surface and a satisfactory degree of agglomeration. The prepared micro-roughness of the etched ceramic would provide an improved surface of the material either for its next step of incorporation into the selected matrix or to directly aid in the attachment and proliferation of osteoblast cells.

Keywords: alumina; zirconia; surface treatment; bioceramics modification; medical applications

1. Introduction

Ceramic biomaterials are widely used in medicine, mainly in orthopedic and dentistry applications [1,2]. This is due to their high hardness, resistance to wear, chemical inertness, lack of inflammatory reaction on the host organisms, their ability to form complex shapes, and aesthetic effects of prostheses, which are important for dental prosthetics [2–4]. Ceramics such as alumina and cubic zirconia are used for acetabulum joints, auditory ossicles, bone scaffolds, dental prostheses (such as crowns), bridges and prosthetic implants, and abutments [5,6]. Ceramics are popular in biomedical applications and allow for the elimination of problems that occur with the use of metal implants, such as metallosis and corrosion, which can cause inflammation, colonization by pathogenic microorganisms, rejection of the implants by the human body, and in extreme cases can lead to cancer [7,8]. The main constituents of dental ceramics are Si-based inorganic materials, such as feldspar, quartz, and silica. Traditional feldspar-based ceramics are also referred to as "Porcelain". The crucial difference between a regular ceramic and a dental ceramic is the proportion

of feldspar, quartz, and silica contained in the ceramic. Because feldspar-based ceramics were prone to failure owing to their inherent brittle nature, ceramics with higher crystalline content such as alumina (aluminium trioxide), Al_2O_3, and zirconia (zirconium dioxide) ZrO_2, were developed to improve the mechanical properties [9].

The adverse effects of metallic implants are associated with the accumulation of harmful metallic ions in detoxification organs [10,11]. Important problems are further associated with inflammation caused by pathogenic microorganisms, most often Candida albicans, Typhylococcus aureus group [12], Aggregatibacter actinomycetemcomitans [13], and Eikenella corrodens. It is assumed that over 65% of all human infections have been estimated to be biofilm-related [14–16]. Bacterial and fungal inflammations, and their related issues, are the most noticeable in metal biomaterials and alloys [16–18]. Inflammations, and bone loss, are problems that can be avoided with the use of ceramic biomaterials.

Despite the numerous advantages, the application of ceramics brings some issues that arise from the physicochemical nature of this group of materials. This is analogous to the zirconium drawbacks connected with its metastable nature, which a significant amount of work has been dedicated to [19–23]. Other disadvantages of ceramics are their high fragility and a relatively time-consuming and expensive production process, metastable phase's stabilization, and dopant selection [24–29].

There are many ways to develop a sufficiently large surface area on the ceramic surface: oxidation, application of characteristic functional groups, silanization, thermal treatment in a gas atmosphere, melt infiltration, ionic liquid etching, sol-gel process, and co-precipitation [30–35]. For example, the chemical etching processes have a large amount of literature focused on chemical etching concerns for the preparation of the ZrO_2 surface in a way that enables permanent bonding to hard dental tissues or composite materials [35]. One of the important aspects required for the success of ZrO_2 ceramics is the establishment of proper adhesion between substrate and adherent. The gold-standard protocol for resin bonding to glass-ceramics is etching with hydrofluoric acid, followed by the application of a silane coupling agent (chemical and mechanical adhesion) [35,36]. Acid etching applying various concentration and times has been shown to change the surface micro-morphology of glass and oxide ceramics with many surface defects. The resin adhesion, the increase of HF concentration, and the etching time is responsible for the increase of the surface area available to adhesion with resin [35].

The morphology study effect via micro-roughness of etched ceramics is important for further application and next step incorporation into the selected matrix or directly helps the osteoblast cell attachment and proliferation [37–39]. Morphology roughness is important for other inorganic modifications; e.g., precipitation of apatite ceramics [40–42].

Here, we report a simple and low-cost surface modification process for medical-grade ZrO_2 and Al_2O_3 ceramics using chemical acids. This treatment was carried out to prepare surface of ceramic fillers for a further modification or for incorporation into selected matrix. For the etching process, we used sulphuric acid, nitric acid, peroxide, and hydrofluoric acid. The performed research concerns the assessment of the impact of prepared etching baths on the surface development, chemical and phase composition.

2. Materials and Methods

2.1. Samples Preparation

The test samples were prepared from ceramic powders of alumina (Al_2O_3 99.9%, CAS 1344-28-1, Sigma Aldrich/Merck KGaA, Darmstadt, Germany) and zirconia (ZrO_2 99% purity excludes ~2% HfO_2, CAS 1314-23-4, Sigma Aldrich/Merck KGaA, Darmstadt, Germany).

Concentrated Sulphuric acid 98% H_2SO_4 (CAS 7664-93-9), nitric acid 65%HNO_3 (CAS 7697-37-2), hydrofluoric acid HF (CAS 7664-39-3) and hydrogen peroxide (CAS 7722-84-1) 35% H_2O_2. All reagents were purchased from Avantor Chemicals, Radnor, PA, USA. The samples were prepared in 3 g batches. Powder samples without any pre-treatment were chemically etched in the following solutions: (I) hot, fresh Piranha solution (98%

H_2SO_4 + 35% H_2O_2), (II) sulphuric 98% H_2SO_4 and nitric 65% HNO_3 acid mixture, and (III) hydrofluoric acid 45% HF.

The work with all concentrated acids and their mixtures are dangerous and relevant precautions must be applied. Acid resistant protective clothing and gloves and safety goggles or a combination of safety goggles and a face shield where splashing is a possibility is recommended.

The sample names, process times, and etching baths are given in Table 1.

Table 1. All sample's experimental conditions and description for both ceramic samples.

Agent, Cp%	Etching Time, (s)	Concentration Cp%	Sample Name ALUMINA	Sample Name ZIRCONIA
98% H_2SO_4: 35% H_2O_2	60	100	ZrO2_PS1_60	Al2O3_PS1_60
	120		ZrO2_PS1_120	Al2O3_PS1_120
98% H_2SO_4: 65% HNO_3 1:3	60	100	ZrO2_SN1_60	Al2O3_SN1_60
	120		ZrO2_SN1_120	Al2O3_SN1_120
45% HF	60	15	ZrO2_HF0.15_60	Al2O3_HF0.15_60
	120		ZrO2_HF0.15_120	Al2O3_HF0.15_120

Note: key for sample name: ceramics _ abbreviation of etching agent with concentration _ etching time.

The ceramic powder samples were placed in a beaker with an etching solution and mixed with a magnetic stirrer. The time of etching was set to 60 s and 120 s. After etching, the samples were quantitatively transferred to a paper filter and washed with deionized water (3 × 200 cm^3) and filtered under pressure through filter with a ceramic membrane to remove the remaining etching solution. The samples were then transferred to a dryer and dried at natural airflow at 80 °C for 24 h. After cooling the samples were added to a beaker with 2-propanol (Merck KGaA, Darmstadt, Germany) and placed in an ultrasonic bath to homogenize them for 15 min. The samples were then again transferred to a dryer and dried at natural airflow at 80 °C for 24 h. The samples thus prepared were then used to characterize the materials.

2.2. Characterization

The prepared samples were tested in terms of their morphology, phase composition and structure, chemical composition, and specific surface development. The morphology and initial elemental composition analysis using Scanning Electron Microscopy JEOL JSM-7610F+ (JEOL, Tokyo, Japan) with Schottky cathode equipped with energy-dispersive X-ray spectroscopy Aztec Ultima Max 65 (Oxford Instruments, Abingdon, UK) (SEM/EDS) were performed. Both secondary and back scattered electrons regimes were employed to take the best electron micrographs of area of interests and EDS mapping was applied to uncover elemental composition. Samples were placed on the stubs covered with carbon tape and coated with platinum (20 nm) to reach best resolution and avoid possible charging.

The analysis of characteristic bonding interactions using Fourier transform infrared (FTIR) spectroscopy was performed. The FTIR spectra of all samples were measured using the attenuated total reflectance technique. The samples were pressed using a pressure device on the single-reflection diamond crystal, and spectra were collected using an FT-IR Nicolet iS50 (Thermo Scientific, Waltham, MA, USA) spectrometer with a Smart Orbit ATR accessory and a deuterated triglycine sulphate detector. The measurement conditions were as follows: spectral region = 4000–400 cm^{-1}; spectral resolution = 4 cm^{-1}; 64 scans; Happ-Genzel apodisation.

The X-ray powder diffraction (XRD) analysis was performed using a RIGAKU Ultima IV diffractometer (Rigaku, Tokyo, Japan), with a scintillation detector, CuKα radiation source, NiKβ filter, and Bragg-Brentano arrangement. Samples were measured in ambient

atmosphere using reflexion mode (conditions: 40 kV, 40 mA, 2°/min, 0.05 step). The database used for qualitative phase analysis was ICDD PDF-2/Release 2011 RDB.

Specific surface was determined via nitrogen adsorption/desorption isotherms, which were measured using Autosorb (Quantachrome Instruments iQ2, Boynton Beach, FL, USA). Prior to the analysis, all samples were degassed for 3.6 h at 300 °C. The specific surface area was calculated using the Brunauer–Emmett–Teller (BET) method. Porosity and pore size distribution was determined using the Barrett–Joyner–Halenda (BJH) method, applying the software from the producer of the apparatus. Approximate pore shapes were specified based on de Boer adsorption hysteresis classification.

3. Results and Discussion

3.1. Morphology Evaluation and Elements Mapping of the Surface

One of the most important approaches in our study was to characterize the surface of studied ceramics after acid etching. Microscopy observations allowed determining morphology changes and agglomeration of ceramic particles caused by acidic etching. In addition, EDS measurements confirmed the chemical composition of the selected areas of interest.

The initial powders of alumina and zirconia are shown in Figure 1.

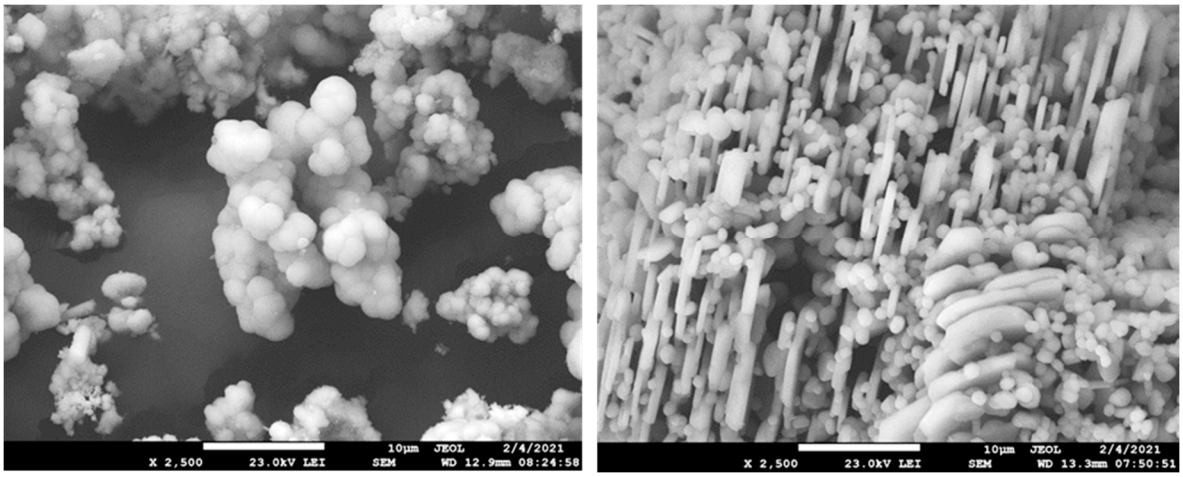

Figure 1. SEM pictures of original powders of zirconia (**left**) and alumina (**right**).

Zirconia ceramics has round particles of non-uniform particle size. Based on SEM observation the individual spheres are in range 1–5 µm. All particles are fused to form stable agglomerates. Contrary to ZrO_2 the alumina is exposing small platelet-like particles morphology surrounded with small round particles. The size of the particles can be approximated to be 10 µm as the longest diameter and less than 1 µm as the shortest.

The microscopy study focuses on the morphology and shapes of ceramic particles, and on particles interactions. Here, we can evaluate the state of interacting particles. The aggregation of particles is understood through the process of classical nucleation, growth, collision, and attachment, where aggregated particles form among the generated concrete nano particles. The route to form agglomerated particles is through cluster aggregation, nucleation, and growth. Then, the agglomerated particles are generated from atomic clusters of different components, but eventually form particles with uniform components.

Additionally, the force among particles in aggregation and agglomeration is different because the direct force among particles caused by aggregation is a van der Waals force, but the force existing in agglomerated particles is due to chemical bonding such as hydrogen bonding, which is much stronger than the force in aggregated particles. The final shape of the inorganic nano particles resulting from aggregation and agglomeration is different. The shape caused by aggregation is an undefined one, whereas the shape caused by agglomeration is usually spherical.

Furthermore, the general size of the particles generated by agglomeration is on the micro-scale. We expect the particles to be agglomerated rather than only aggregated in our case of chemical etching since the particles of ceramics are appearing compact and it is not easy to disintegrate via simple laboratory mechanical approaches.

The zirconia samples displayed a general tendency to agglomerate independently on the etching agent, and there are no significant differences between concentration and etching time. Among all etching agents, the largest degrees of agglomeration were observed when using a mixture of sulphuric and nitric acids, and we could observe stable agglomerates about 30 µm regularly. The lowest agglomeration noted following the use of hydrofluoric acid where brittle agglomerates are visible. The variability of the agglomerates is presented on Figure 2.

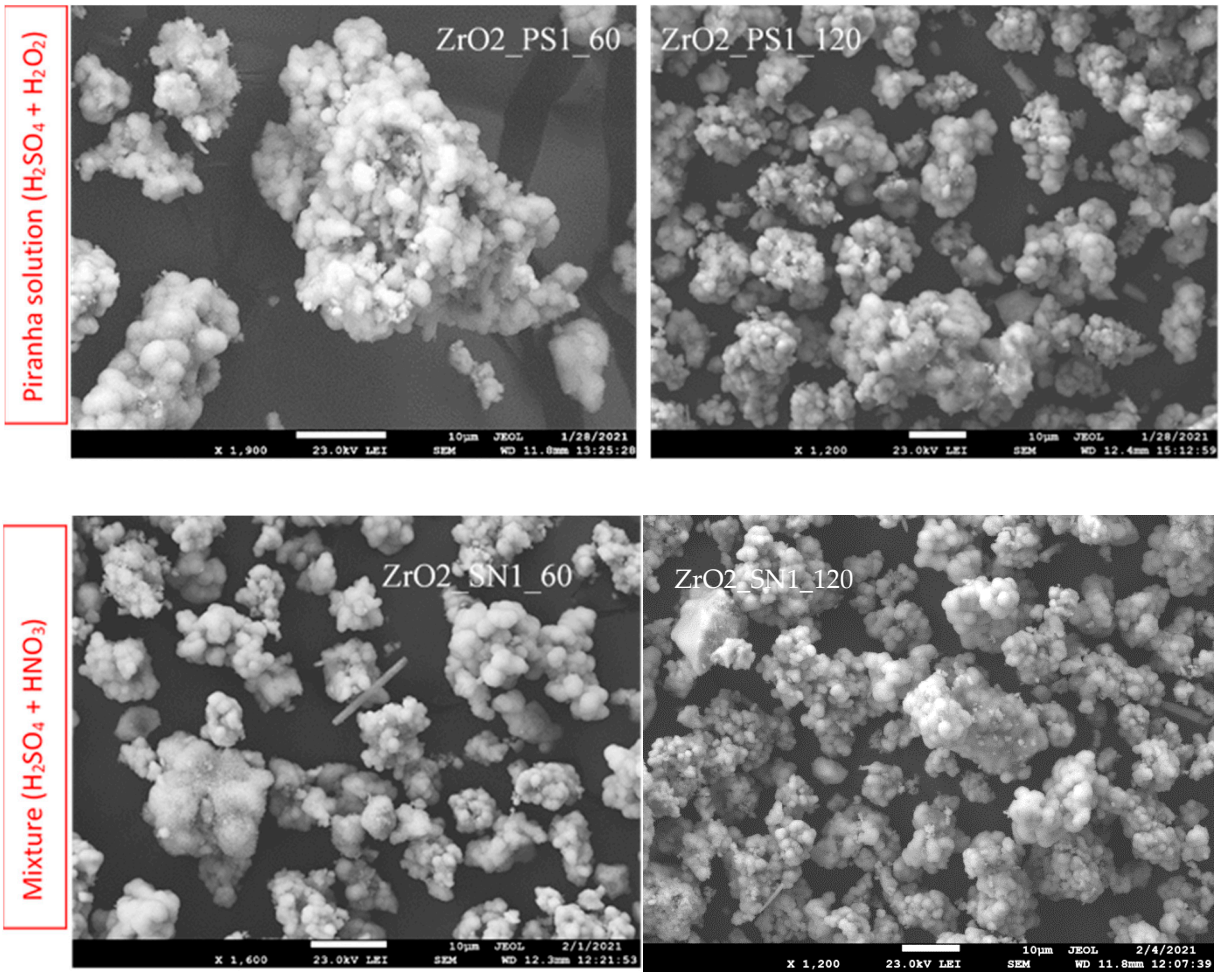

Figure 2. *Cont.*

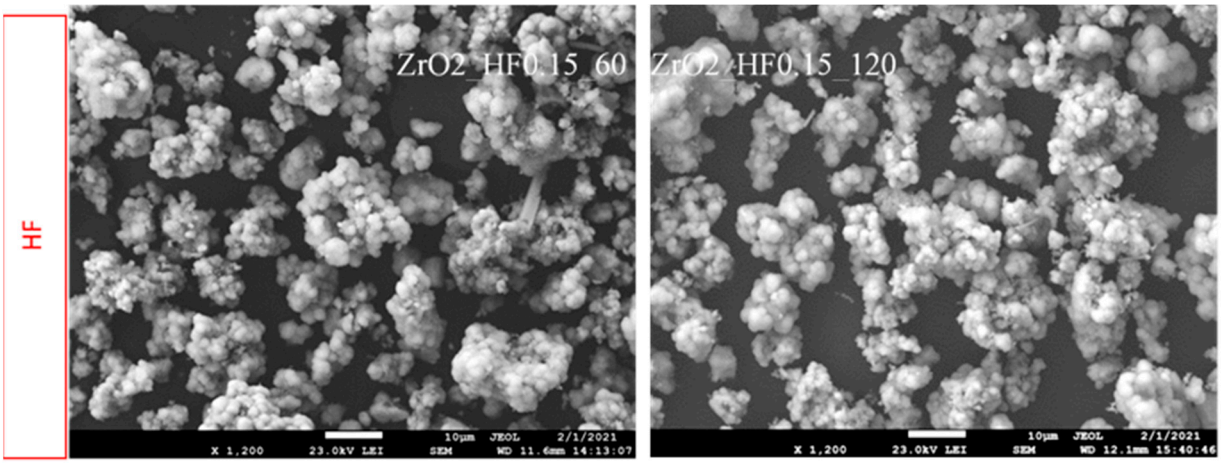

Figure 2. SEM images comparing the degree of agglomeration of zirconia powders after etching with different acids.

In general, less agglomeration was observed in alumina samples Figure 3, because these powders were more dispersed and therefore less susceptible to agglomeration. However, the dependence of alumina agglomeration on the etching agent was similar to that observed for the zirconia samples. Specifically, most alumina agglomerates were observed at treatments with a mixture of sulphuric and nitric acid, while less were observed for hydrofluoric acid, and the least for Piranha solution.

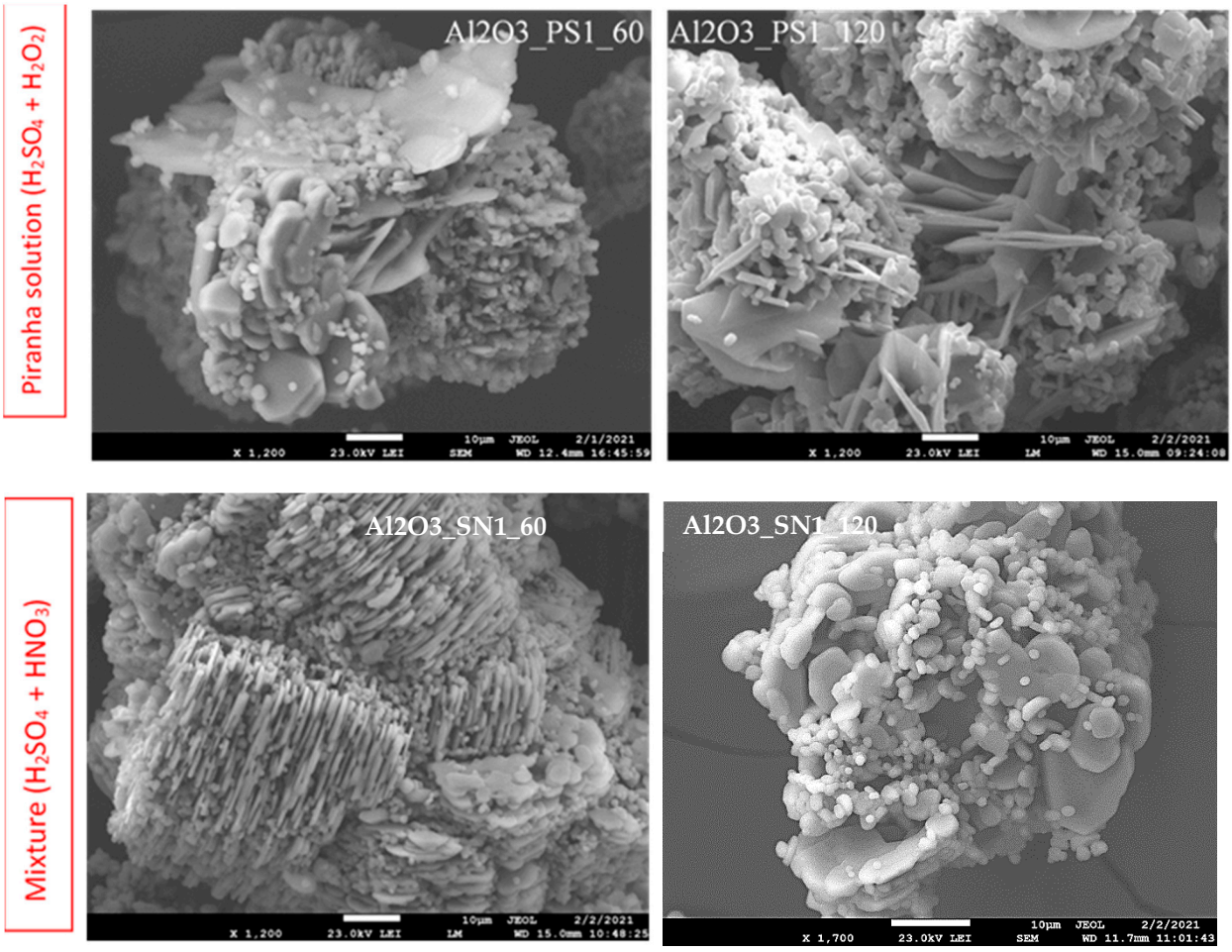

Figure 3. *Cont.*

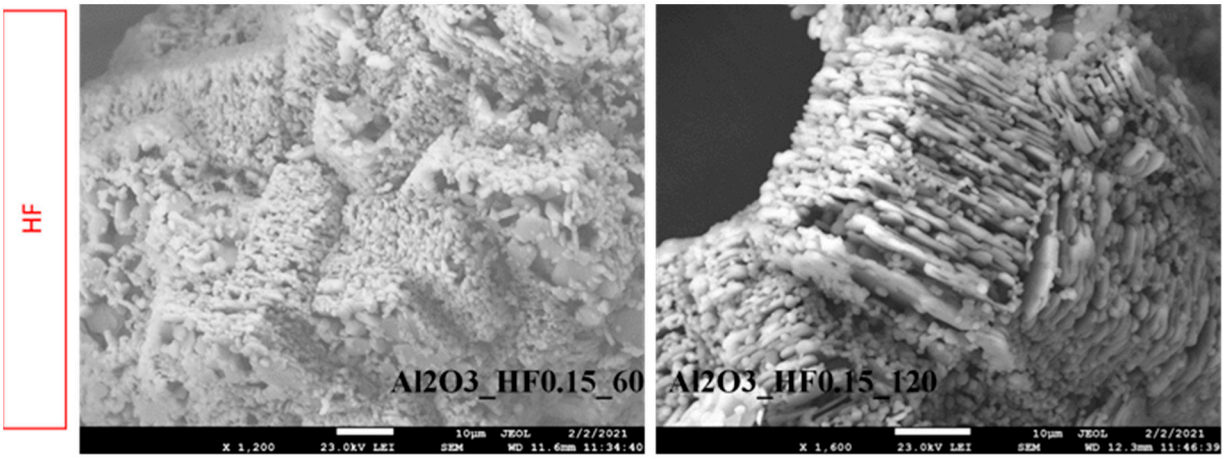

Figure 3. SEM images comparing the degree of agglomeration of alumina powders after etching with different acids.

For observation of the changes in chemical composition of surfaces, the EDS mapping was employed. All combination of etching was checked, and case samples are shown in Figures 4 and 5.

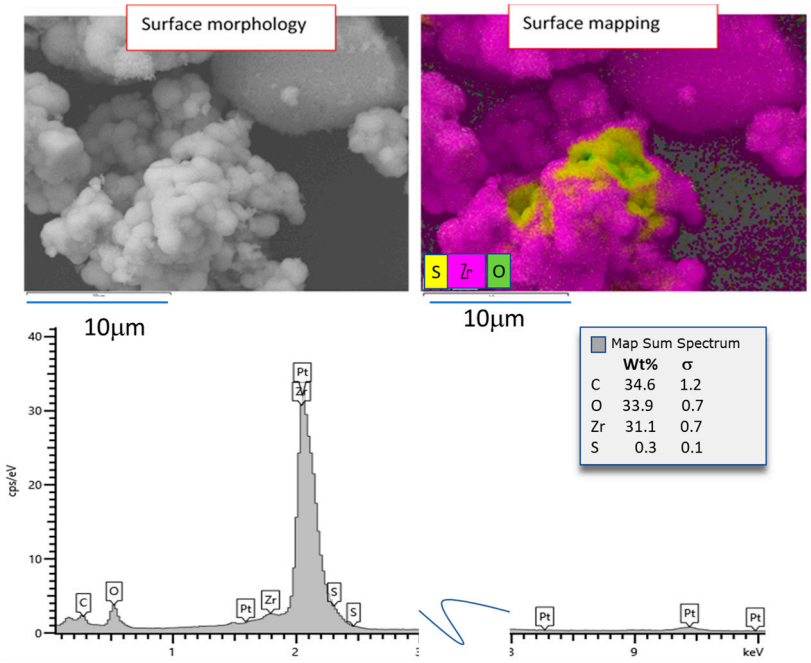

Figure 4. Chemical analysis of example ZrO2_PS sample using EDS mapping (detected C is background from mounting carbon tape, Pt is conductive coating).

Observing the zirconia surface, places with certain concentrations of sulphur were found; however, the amount in total was not higher than 0.5 wt%. Other elements, except original ceramics, were not found on the surface of zirconia. Only the samples treated with Piranha solution had the traces of sulphur that was not visibly crystalline Figure 4. The remainder of the samples was not enriched with other elements.

A different situation lies in the case of alumina ceramics (Figure 5). The visibly crystalline phase of sulphur compound is detected at EDS mapping, where smooth and flat crystals of other phase are ingrowth to the fine grains of alumina ceramics. The sulphur compound's crystals seem to be arranged randomly; however, some of them are placed often on the edges of alumina agglomerate or creating bridge so that particles are joined together.

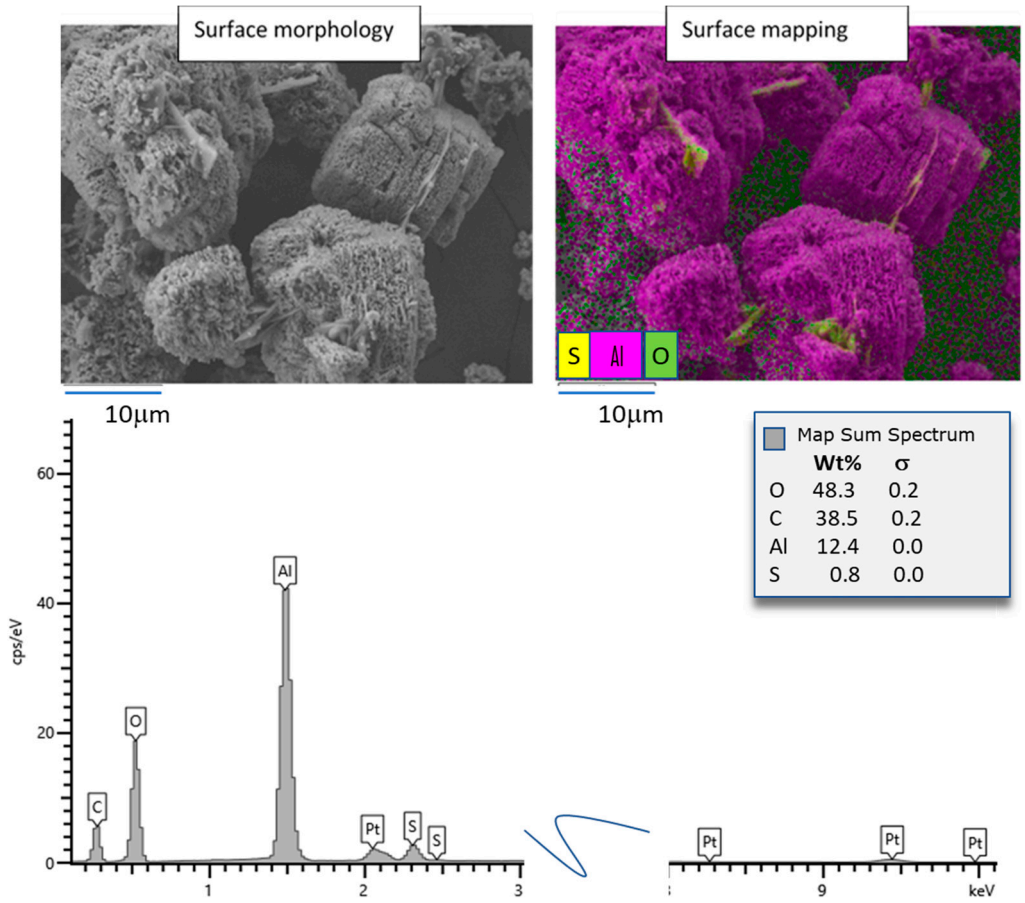

Figure 5. Chemical analysis of example Al2O3_PS sample using EDS mapping (detected C is background from mounting carbon tape, Pt is conductive coating).

Evaluating the elemental composition of the map we can presume that the crystals are sulphate, which is later confirmed via XRD analysis as $Al(HSO_4)_3 \cdot 6H_2O$.

The observation of the microstructure of zirconia powders led to the clear conclusion that they were most altered in the Piranha solution environment, while the intensity of morphology disturbance corresponded to the concentration of reagents and the time of contact.

The situation was similar after etching alumina samples with a mixture of sulphuric and nitric acid, although these surfaces were etched to a lesser degree than those subjected to Piranha solution.

3.2. Structural Characterization of Etched Samples

The FTIR spectra for all selected samples are shown in Figure 6. For zirconia samples etched in Piranha solution ZrO2_PS1_120 and ZrO2_PS1_60, several characteristic bands were identified. The absorption bands that appear at 1633, 1031, and 1030 cm^{-1} are related to the vibration, stretching, and deformation of the O–H bonds present due to absorption and coordination of water in the samples. The peaks at 1088 (1089) cm^{-1} result from the bending vibrations of hydroxyl groups bound to zirconium oxide. However, the absorption bands at 724(725), 485, 482, 447, and 444 cm^{-1} correspond to Zr-O bond vibrations in both zirconia samples [35,36]. Zirconia sample ZrO2_PS1_60 FTIR spectrum contains characteristic absorption bands at 722 and 483 cm^{-1}, which are associated with the Zr-O bending vibration [42–44]. In addition, it was determined that the bands at 450–550 cm^{-1} and 750–950 cm^{-1} correspond to tetragonal zirconia. The monoclinic phase cannot be determined decisively from the FTIR spectrum [35]. Samples etched in hydrofluoric acid exhibited bands at 721, 485 (486), and 447 cm^{-1}, which all originate from bending vibrations

of Zr-O [42–45]. The band at 666 cm^{-1} is due to fluoride adsorption. For alumina etched in Piranha solution, the bands at 2984 and 2979 cm^{-1} were identified as being associated with Al_2O_3 stretching vibrations, along with those in the region of 2950–2850 cm^{-1} (which are not shown in the spectra in Figure 6). This is likely due to so-called "bulk-like" droplets in the pores, or a thin film adsorbed on the surface of the alumina. Other bands observed at 634, 555, 551, 494, and 406 cm^{-1} are associated with the bending vibrations of Al-O and Al-O-Al in the γ-Al_2O_3 and Al-O-H moieties [44]. The alumina sample etched with a mixture of sulphuric and nitric acid had characteristic absorption bands at 589, 416, and 412 cm^{-1}, corresponding approximately to the range previously determined to contain Al-O and Al-O-Al bending motions within γ-Al_2O_3 and Al-OH [46]. The FTIR spectra for alumina samples etched with hydrofluoric acid were interpreted similar to the spectrum of alumina sample etched with the mixture of sulphuric and nitric acid.

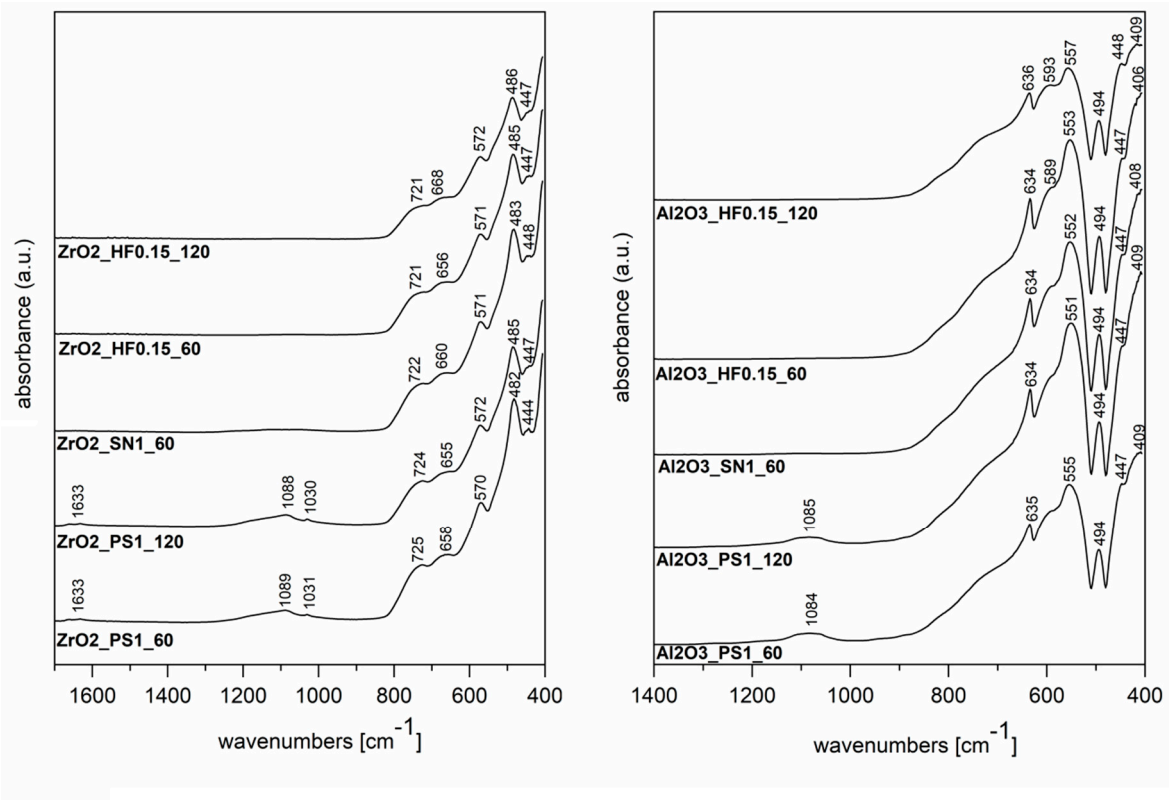

(**a**) (**b**)

Figure 6. FTIR spectra of modified samples with denoted most intensive bands (**a**) samples of zirconia ceramics, (**b**) samples of alumina ceramics.

Evaluation of the structure and changes at the etching process was performed using XRD measurements, and a summary of samples diffractograms is presented in Figures 7 and 8.

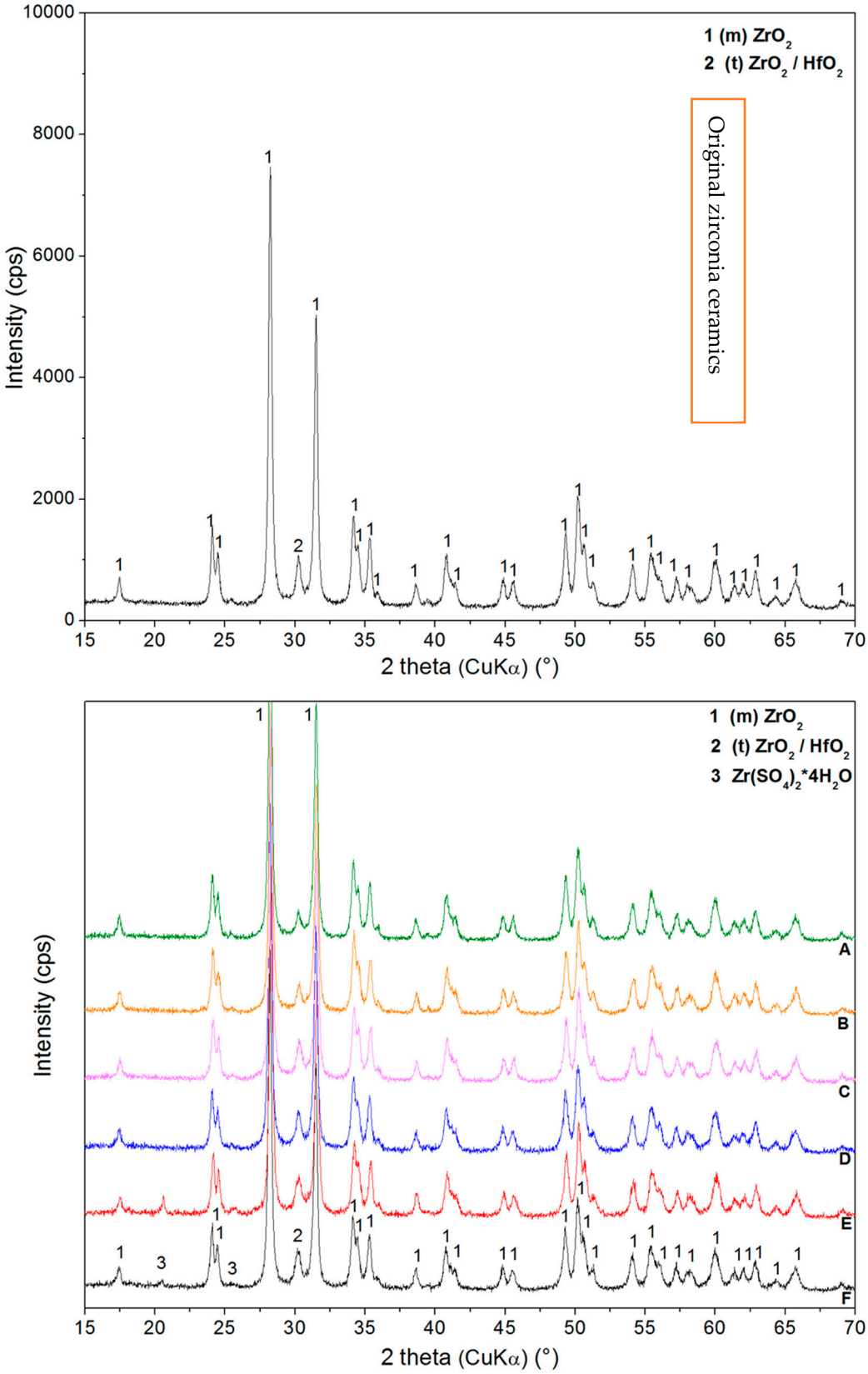

Figure 7. XRD patterns for zirconia: as received sample (**top**) and modified samples (**bottom**): (**A**) ZrO2_HF0.15_120; (**B**) ZrO2_HF0.15_60; (**C**) ZrO2_SN1_120; (**D**) ZrO2_SN1_60; (**E**) ZrO2_PS1_120; (**F**) ZrO2_PS1_60; where peaks of evaluated phases are mentioned in the pattern.

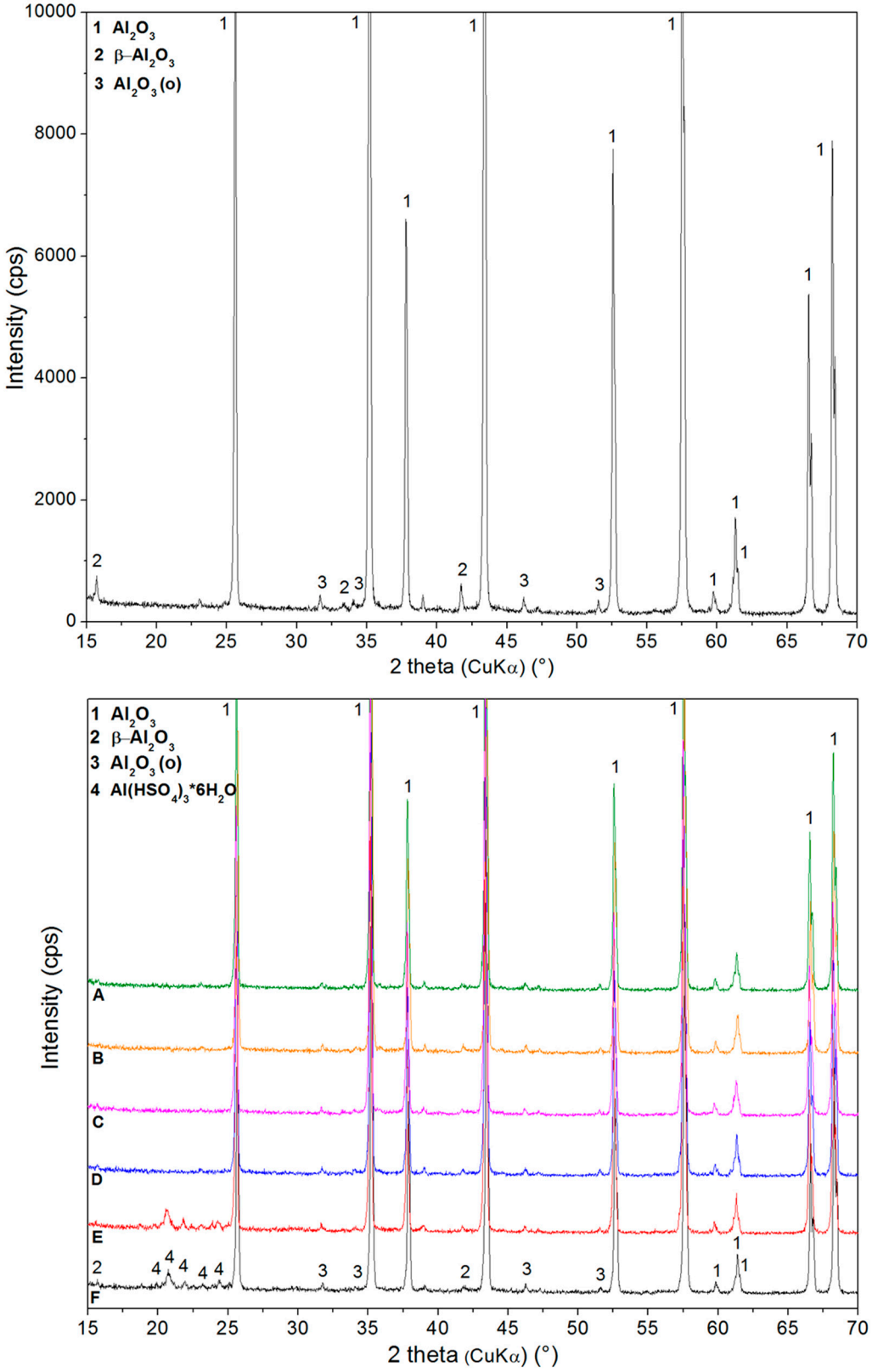

Figure 8. XRD patterns for alumina: as received sample (**top**) and modified samples (**bottom**). (**A**) Al2O3_HF0.15_120; (**B**) Al2O3_HF0.15_60; (**C**) Al2O3_SN1_120; (**D**) Al2O3_SN1_60; (**E**) Al2O3_PS1_120; (**F**) Al2O3_PS1_60; where peaks of evaluated phases are mentioned in the pattern.

3.3. Specific Surface Area and Porosity Evaluation

To evaluate the surface of etched ceramics the porosity measurement and specific surface area (SSA) analysis (Figure 9) was employed. Treatment of the ceramics with Piranha solution and HF acid was evaluated. Table 2 presents the data of measured specific surface area, porosity, and pore volume of selected samples. In general, the zirconia samples underwent greater surface development than alumina after etching with any of the respective acids tested herein. As for zirconia, the samples' pore volumes tended to be greater than 0.4 cm^3g^{-1}, which indicates more opportunity for further modification or embedding in selected matrix. Similar tendency is visible in the case of SSA, ZrO_2 particles are representing larger SSA than the Al_2O_3 surface. The alumina samples in this study exhibited a lesser degree of surface development in each case. This can be explained by the fact that the initial zirconia has a lower susceptibility to etching and greater fineness than the original alumina. In the case of sample ZrO2_HF0.15_120 (Table 2), no reliable pore data was obtained to allow comparison to other samples. Measurement of the ceramic samples after H_2SO_4/HNO_3 treatment was not possible to perform using available device, due to very small undetectable SSA.

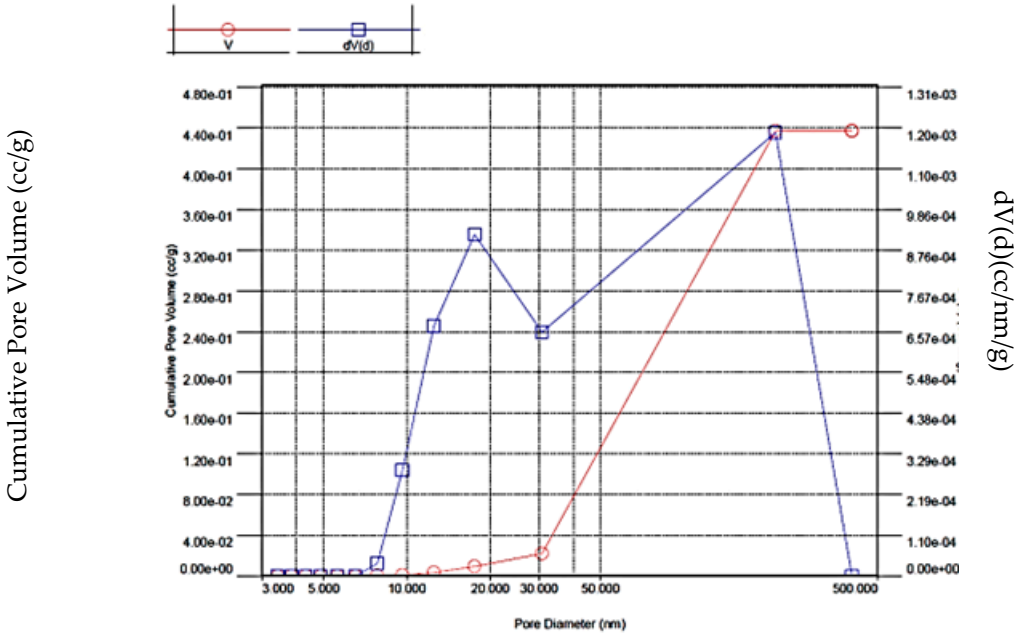

Figure 9. Example of BJH plots for zirconia sample ZrO2_PS1_60.

Table 2. Surface area development, pore volumes, and pore diameters.

Powder	Sample	Specific Surface Area, [m^2g^{-1}]	Pore Volume, [cm^3g^{-1}]	Pore Diameter, [nm]
Zirconia	ZrO2_PS1_60	11.842	0.437	214.681
	ZrO2_PS1_120	7.369	0.072	17.658
	ZrO2_HF0.15_60	13.455	0.425	183.673
	ZrO2_HF0.15_120	12.745	0.431	206.289
Alumina	Al2O3_PS1_60	3.543	0.165	186.250
	Al2O3_PS1_120	0.220	0.006	3.069
	Al2O3_HF0.15_60	0.316	0.008	3.817
	Al2O3_HF0.15_120	0.610	n.d.	n.d.

n.d.—not possible to obtain data.

4. Conclusions

Medical grade zirconia and alumina were treated in 3 types of etching agents. For this purpose, three etching agents were used: (I) fresh hot Piranha solution, (II) a mixture of 98% H_2SO_4 and 65% HNO_3 acids, and (III) 45% hydrofluoric acid. Based on the observed morphologies, and the chemical and phase composition studies, the following relationships were elucidated. The most changed morphology of the ceramic surfaces was observed in case zirconia treated with Piranha solution, whereas the H_2SO_4/HNO_3 solutions had the least influence on surface changes. In the case of HF, the effect is indirect. Depending on the acid's oxidation power, different degrees of agglomeration were introduced, and as the oxidation power decreased, the least agglomeration was observed (using HF in both zirconia and alumina samples). Regardless of the acid used, a larger extent of agglomeration was always observed in zirconia, relative to alumina. Based on BET specific surface area measurements and their correlation with SEM results, the highest specific surface development was observed for zirconia etched in HF and slightly lower values were obtained after using Piranha solution. For alumina, the BET results revealed a more complicated relationship. Since these ceramic powders were already larger than zirconia, the alumina tiles were broken down into agglomerates, and it was difficult to disintegrate them. The sulphur impurities were detected in samples etched with Piranha solution. Phase analysis using XRD found phases of hydrated sulphate compounds, especially Al_2O_3 particles which were decorated with micrometers of large, hydrated $Al(HSO_4)_3$ crystals. In case of zirconia, it is only amorphous coating.

The findings of the articles are important for next step in fabrication of composite implants in the dentistry and/or other prosthetics. The potential of surface modification to make zirconia or alumina a successful implant material in the future is highly dependent on the establishment of successful in in-vitro and in-vivo studies [47,48] and various body fluids' stability [49]. Hence, further effort should be made in order to deepen the understanding of tissue response to the implant and tissue regeneration processes.

Author Contributions: Conceptualization, D.S.N.; methodology, G.S.M. and D.S.N.; validation, G.K, G.S.M.; formal analysis, M.H., S.H., J.M., P.K. and G.K.; investigation, D.S.N.; data curation, S.H., M.H.; writing—original draft preparation, D.S.N., M.H. and G.S.M.; writing—review and editing, G.S.M., M.H., G.K., S.K.S. and D.S.N.; supervision, Z.P.; project administration, M.H.; funding acquisition, G.S.M. and A.S. All authors have read and agreed to the published version of the manuscript.

Funding: This work was supported by the ESF in "Science without borders" projects CZ.02.2.69/0.0./0.0./16_027/0008463 within the Operational Programme Research, Development and Education, Ministry of Education, Youth and Sport of the Czech Republic SP2021/106 and SP2021/90. New technological solutions for 3d printing of metals and composite materials, CZ.02.1.01/0.0/0.0/17_049/0008407 financed by ESF. Dotation of Polish Ministry of Science and Higher Education 07/020/BK_21/0067 (BK-293/RIB3/2021).

Data Availability Statement: Additional data not published in the article can be provided by corresponding author upon request.

Conflicts of Interest: The authors declare no conflict of interest.

References

1. Afewerki, S.; Bassous, N.; Harb, S.; Palo-Nieto, C.; Ruiz-Esparza, G.U.; Marciano, F.R.; Webster, T.J.; Furtado, A.S.A.; Lobo, A.O. Advances in dual functional antimicrobial and osteoinductive biomaterials for orthopaedic applications. *Nanomedicine* **2020**, *24*, 102143. [CrossRef]
2. Kargozar, S.; Ramakrishna, S.; Mozafari, M. Chemistry of biomaterials: Future prospects. *Curr. Opin. Biomed. Eng.* **2019**, *10*, 181–190. [CrossRef]
3. Nakonieczny, D.S.; Ziębowicz, A.; Paszenda, Z.K.; Krawczyk, C. Trends and perspectives in modification of zirconium oxide for a dental prosthetic applications–A review. *Biocyber. Biomed. Eng.* **2017**, *37*, 229–245. [CrossRef]
4. Piconi, C.; Maccauro, G. Zirconia as a ceramic biomaterial. *Biomaterials* **1999**, *20*, 1–25. [CrossRef]
5. Sanon, C.; Chevalier, J.; Douillard, T.; Cattani-Lorente, M.; Scherrer, S.S.; Gremillard, L. A new testing protocol for zirconia dental implants. *Dent. Mater.* **2015**, *31*, 15–25. [CrossRef] [PubMed]

6. Ferrari, M.; Vichi, A.; Zarone, F. Zirconia abutments and restorations: From laboratory to clinical investigations. *Dent. Mater.* **2015**, *31*, e63–e76. [CrossRef] [PubMed]
7. Cheng, F.T.; Shi, P.; Man, H.C. Nature of oxide layer formed on NiTi by anodic oxidation in methanol. *Mater. Lett.* **2005**, *59*, 1516–1520. [CrossRef]
8. Jin, W.; Wang, G.; Qasim, A.M.; Mo, S.; Ruan, Q.; Zhou, H.; Li, W.; Chu, P.K. Corrosion protection and enhanced biocompatibility of biomedical Mg-Y-RE alloy coated with tin dioxide. *Surf. Coat. Tech.* **2019**, *357*, 78–82. [CrossRef]
9. Ho, G.W.; Matinlinna, J.P. Insights on Ceramics as Dental Materials. Part I: Ceramic Material Types in Dentistry. *Silicon* **2011**, *3*, 109–115. [CrossRef]
10. Sullivan, S.J.L.; Madamba, D.; Siva, S.; Miyashiro, K.; Dreher, M.L.; Trépanier, C.; Nagaraja, S. The effects of surface processing on in-vivo corrosion of Nitinol stents in a porcine model. *Acta Biomater.* **2017**, *62*, 385–396. [CrossRef]
11. Talha, M.; Ma, T.; Kumar, P.; Lin, Y.; Singh, A. Role of protein adsorption in the bio corrosion of metallic implants-A review. *Coll. Surf. B Biointer.* **2019**, *176*, 494–506. [CrossRef] [PubMed]
12. Bapat, A.; Chaubal, T.V.; Joshi, C.P.; Bapat, P.R.; Choudhury, H.; Pandey, M.; Gorain, B.; Kesharwani, P. An overview of application of silver nanoparticles for biomaterials in dentistry. *Mater. Sci. Eng. C* **2018**, *91*, 881–898. [CrossRef]
13. Noronha, V.T.; Paula, A.J.; Duran, G.; Galembeck, A.; Cogo-Müller, K.; Franz-Montan, M.; Durán, N. Silver nanoparticles in dentistry. *Dent. Mater.* **2017**, *33*, 1110–1126. [CrossRef] [PubMed]
14. Pazourková, L.; Reli, M.; Hundáková, M.; Pazdziora, E.; Predoi, D.; Simha Martynková, G.; Lafdi, K. Study of the Structure and Antimicrobial Activity of Ca-Deficient Ceramics on Chlorhexidine Nanoclay Substrate. *Materials* **2019**, *12*, 2996. [CrossRef]
15. Garcia Silva-Bailão, M.; Lobato Potenciano da Silva, K.; Raniere Borges Dos Anjos, L.; de Sousa Lima, P.; de Melo Teixeira, M.; Maria de Almeida Soares, C.; Melo Bailão, A. Mechanisms of copper and zinc homeostasis in pathogenic black fungi. *Fung. Biol.* **2018**, *122*, 526–537. [CrossRef] [PubMed]
16. de Avila, E.D.; Castro, A.G.B.; Tagit, O.; Krom, B.P.; Löwik, D.; van Well, A.A.; Bannenberg, L.J.; Vergani, C.E.; van den Beucken, J.J.J.P. Anti-bacterial efficacy via drug-delivery system from layer-by-layer coating for percutaneous dental implant components. *Appl. Surf. Sci.* **2019**, *488*, 194–204. [CrossRef]
17. Uhlmann, E.; Schweitzer, L.; Kieburg, H. The Effects of Laser Microtexturing of Biomedical Grade 5 Ti-6Al-4V Dental Implants (Abutment) on Biofilm Formation. *Procedia* **2018**, *68*, 184–189. [CrossRef]
18. Frutos, E.; Alvares, D.; Fernandez, L.; González-Carrasco, J.-L. Effects of bath composition and processing conditions on the microstructure and mechanical properties of coatings developed on 316 LVM by hot dipping in melted AlSi alloys. *J. Alloy. Comp.* **2014**, *617*, 646–653. [CrossRef]
19. Chevalier, J.; Gremillard, L.; Virkar, A.; Clarke, D.R. The Tetragonal-Monoclinic Transformation in Zirconia: Lessons Learned and Future Trends. *J. Am. Ceram. Soc.* **2009**, *92*, 1901–1920. [CrossRef]
20. Graziani, G.; Barbaro, K.; Fadeeva, I.V.; Ghezzi, D.; Fosca, M.; Sassoni, E.; Vadalà, G.; Cappelletti, M.; Valle, F.; Baldini, N.; et al. Ionized jet deposition of antimicrobial and stem cell friendly silver-substituted tricalcium phosphate nanocoatings on titanium alloy. *Bio. Mater.* **2021**, *6*, 2629–2642.
21. Guo, X. Property Degradation of Tetragonal Zirconia Induced by Low-Temperature Defect Reaction with Water Molecules. *Chem. Mater.* **2004**, *16*, 3988–3994. [CrossRef]
22. Gremillard, L.; Melle, S.; Chevalier, J.; Zhao, J.; Fridrici, V.; Kapsa, P.; Geringer, J.; Uribeet, J. Degradation of Bioceramics. In *Degradation of Implant Materials*; Eliaz, N., Ed.; Springer: New York, NY, USA, 2012; pp. 195–252.
23. Nakonieczny, D.S.; Basiaga, M.; Sambok, A.; Antonowicz, M.; Paszenda, Z.K.; Ziębowicz, A.; Krawczyk, C.; Ziębowicz, B.; Lemcke, H.; Kałużyński, P. Ageing of Zirconia Dedicated to Dental Prostheses for Bruxers Part 1: Influence of Accelerating Ageing for Surface Topography and Mechanical Properties. *Rev. Adv. Mater. Sci.* **2019**, *58*, 189–194. [CrossRef]
24. Fan, J.; Lin, T.; Hu, F.; Yu, Y. Effect of sintering temperature on microstructure and mechanical properties of zirconia-toughened alumina machinable dental ceramics. *Ceram. Int.* **2017**, *43*, 3647–3653. [CrossRef]
25. Fornabio, M.; Reveron, H.; Adolfssin, E.; Montanaro, L.; Chevalier, R.; Palmero, P. Design and development of dental ceramics: Examples of current innovations and future concepts. In *Advances in Ceramic Biomaterials-Materials, Devices and Challenges*, 1st ed.; Palmero, P., Cambier, F., de Barra, E., Eds.; Woodhead Publishing: Sawston, UK, 2017; Volume 11, pp. 355–389.
26. Nakonieczny, D.S.; Sambok, A.; Antonowicz, M.; Basiaga, M. Ageing of Zirconia Dedicated to Dental Prostheses for Bruxers Part 2: Influence of Heat Treatment for Surface Morphology, Phase Composition and Mechanical Properties. *Rev. Adv. Mater. Sci.* **2019**, *58*, 218–225. [CrossRef]
27. Istrate, B.; Rau, J.V.; Munteanu, C.; Antoniac, I.V.; Saceleanu, V. Properties and in vitro assessment of ZrO2-based coatings obtained by atmospheric plasma jet spraying on biodegradable Mg-Ca and Mg-Ca-Zr alloys. *Ceram. Int.* **2020**, *46*, 15897–15906. [CrossRef]
28. Nakonieczny, D.S.; Walke, W.; Majewska, J.; Paszenda, Z. Characterization of magnesia-doped yttria-stabilized zirconia powders for dental technology applications. *Acta Bio. Biomech.* **2014**, *16*, 99–106.
29. Nakonieczny, D.S.; Antonowicz, M.; Paszenda, Z.; Radko, T.; Drewniak, S.; Bogacz, W.; Krawczyk, C. Experimental investigation of particle size distribution and morphology of alumina-yttria-ceria-zirconia powders obtained via sol–gel route. *Biocyber. Biomed. Eng.* **2018**, *38*, 535–543. [CrossRef]
30. Roitero, E.; Ochoa, M.; Anglada, M.; Mücklich, F.; Jiménez Piqué, E. Low temperature degradation of laser patterned 3Y-TZP: Enhancement of resistance after thermal treatment. *J. Europ. Ceram. Soc.* **2018**, *38*, 1742–1749. [CrossRef]

31. Yan, M.; Csik, A.; Yang, C.-C.; Luo, Y.; Fodor, T.; Ding, S.-J. Synergistic reinforcement of surface modification on improving the bonding of veneering ceramics to zirconia. *Ceram. Int.* **2018**, *44*, 19665–19671. [CrossRef]
32. Ilyas, A.; Muhammad, N.; Gilani, M.A.; Vankelecom, I.F.J.; Khan, A.L. Effect of zeolite surface modification with ionic liquid [APTMS][Ac] on gas separation performance of mixed matrix membranes. *Sep. Pur. Technol.* **2018**, *205*, 176–183. [CrossRef]
33. Cremers, V.; Rampelberg, G.; Barhoum, A.; Walters, P.; Claes, N.; de Oliveira, T.M.; Van Assche, G.; Bals, S.; Dendooven, J.; Detavernier, C. Oxidation barrier of Cu and Fe powder by Atomic Layer Deposition. *Surf. Coat. Technol.* **2018**, *349*, 1032–1041. [CrossRef]
34. Rao, P.K.; Jana, P.; Ahmad, M.I.; Roy, P.K. Synthesis and characterization of zirconia toughened alumina ceramics prepared by co-precipitation method. *Ceram. Int.* **2019**, *45*, 16054–16061. [CrossRef]
35. Monteiro, J.B.; Oliani, M.G.; Guilardi, L.F. Fatigue failure load of zirconia-reinforced lithium silicate glass ceramic cemented to a dentin analogue: Effect of etching time and hydrofluoric acid concentration. *J. Mech. Behav. Biomed. Mater.* **2018**, *77*, 375–382. [CrossRef] [PubMed]
36. Sattabanasuk, V.; Charnchairerk, P.; Punsukumtana, L.; Burrow, M.F. Effects of mechanical and chemical surface treatments on the resin-glass ceramic adhesion properties. *J. Investig. Clin. Dent.* **2017**, *8*, e12220. [CrossRef] [PubMed]
37. Casuccia, A.; Mazzitellia, C.; Monticelli, F.; Toledano, M.; Osorio, R.; Osorio, E.; Papacchini, F.; Ferrari, M. Morphological analysis of three zirconium oxide ceramics: Effect of surface treatments. *Dent. Mater.* **2010**, *26*, 751–760. [CrossRef] [PubMed]
38. Pazourková, L.; Hundáková, M.; Peikertová, P.; Martynková, G. Preparation of calcium-deficient hydroxyapatite particles on vermiculite by precipitation and sonication. *J. Aust. Ceram. Soc.* **2017**, *53*, 775–785. [CrossRef]
39. Šupová, M.; Suchý, T.; Sucharda, Z.; Filová, E.; Kinderen, J.N.L.M.; Steinerová, M.; Bačáková, L.; Martynková, G.S. The comprehensive in vitro evaluation of eight different calcium phosphates: Significant parameters for cell behaviour. *J. Am. Ceram. Soc.* **2019**, *102*, 2882–2904. [CrossRef]
40. Elsaka, S.E. Influence of surface treatments on the surface properties of different zirconia cores and adhesion of zirconia-veneering ceramic systems. *Dent. Mater.* **2013**, *29*, e239–e251. [CrossRef]
41. Karthigeyan, S.; Ravindran, A.J.; Bhat, T.R.R.; Nageshwarao, M.N.; Murugesan, S.V.; Angamuthu, V. Surface Modification Techniques for Zirconia-Based Bioceramics: A Review. *J. Pharm. Bioallied. Sci.* **2019**, *11* (Suppl. 2), S131–S134. [PubMed]
42. Musyarofah, M.; Soontaranon, S.; Limphirat, W.; Triwikantoro; Pratapa, S. XRD, WAXS, FTIR, and XANES studies of silica-zirconia systems. *Ceram. Int.* **2019**, *45*, 15660–15670. [CrossRef]
43. Merle-Méjean, T.; Barberis, P.; Othmane, S.B.; Nardou, F.; Quintard, P.E. Chemical forms of hydroxyls on/in Zirconia: An FT-IR study. *J. Eur. Ceram. Soc.* **1998**, *18*, 1579–1586. [CrossRef]
44. Qian, Z.; Shi, J.L. Characterization of pure and doped zirconia nanoparticles with infrared transmission spectroscopy. *Nanostruct. Mater.* **1998**, *10*, 235–244. [CrossRef]
45. Yakout, S.M.; Hassan, H.S. Adsorption Characteristics of Sol Gel-Derived Zirconia for Cesium Ions from Aqueous Solutions. *Molecules* **2014**, *19*, 9160–9172. [CrossRef] [PubMed]
46. Zhang, H.; Liu, Y.; Zhu, K.; Siu, G.; Xiong, Y.; Xiong, C. Infrared spectra of nanometre granular zirconia. *J. Phys. Condens. Matter* **1999**, *11*, 2035–2042. [CrossRef]
47. Pagano, S.; Lombardo, G.; Balloni, S.; Bodo, M.; Cianetti, S.; Barbati, A.; Montaseri, A.; Marinucci, L. Cytotoxicity of universal dental adhesive systems: Assessment in vitro assays on human gingival fibroblasts. *Toxicol. In Vitro* **2019**, *60*, 252–260. [CrossRef] [PubMed]
48. Goldberg, M.; Gafurov, M.R.; Makshakova, O.N.; Smirnov, V.; Komlev, V.S.; Barinov, S.M.; Kudryavtsev, E.; Sergeeva, N.; Achmedova, S.; Mamin, G.V.; et al. Influence of Al on the structure and in vitro behavior of hydroxyapatite nanopowders. *J. Phys. Chem. B* **2019**, *123*, 9143–9154. [CrossRef] [PubMed]
49. Suchý, T.; Bartoš, M.; Sedláček, R.; Šupová, M.; Žaloudková, M.; Martynková, G.S.; Foltán, R. Various Simulated Body Fluids Lead to Significant Differences in Collagen Tissue Engineering Scaffolds. *Materials* **2021**, *14*, 4388. [CrossRef]